Likelihood Non-Gaussianity in Large Scale Structure Analyses

ChangHoon Hahn, et al.

Lawrence Berkeley National Laboratory, 1 Cyclotron Rd, Berkeley CA 94720, USA

`changhoon.hahn@lbl.gov`

ABSTRACT

abstract here

Subject headings: methods: statistical — galaxies: statistics — methods: data analysis — cosmological parameters — cosmology: observations — large-scale structure of universe

1. Introduction

- Talk about the use of Bayesian parameter inference and getting the posterior in LSS cosmology

- Explain the two major assumptions that go into evaluating the likelihood

- Emphasize that we are not talking about non-Gaussian contributions to the likelihood

- Emphasize the scope of this paper is to address whether one of the assumptions matters for galaxy clustering analyses.

- Depending on Hogg's paper maybe a simple illustration of how the likelihood asumption

However, as we show in this paper, the assumption of likelihood Gaussianity is not necessary. In fact, we will show that the mock catalogs used in standard LSS analyses to estimate the covariance matrix for evaluating the Gaussian likelihood, can be used to quantify the non-Gaussianity. More important the mock catalogs can be used to construct an accurate estimator for the non-Gaussian likelihood.

2. Mock Catalogs

Mock catalogs play an indispensable role in standard cosmological anslyses of LSS studies. They're used for testing analysis pipelines (Beutler et al. 2017; Grieb et al. 2017; Tinker & et al. in preparation), testing the effect of systematics (Guo et al. 2012; Vargas-Magaña et al. 2014; Hahn et al. 2017; Pinol et al. 2017; Ross et al. 2017), and, most relevantly for this

paper, estimating the covariance matrix (Parkinson et al. 2012; Kazin et al. 2014; Grieb et al. 2017; Alam et al. 2017; Beutler et al. 2017; Sinha et al. 2017). In fact, nearly all current state-of-the-art LSS analyses use covariance matrices estimated from mocks to evaluate the likelihood for parameter inference.

While some argue for analytic estimates of the covariance matrix (e.g. Mohammed et al. 2017) or estimates directly from data by subsampling (e.g. Norberg et al. 2009), covariance matrices from mocks have a number of advantages. Mocks allow us to incorporate detailed systematic errors present in the data and variance beyond the volume of the data. Even for analytic estimates, a large ensemble of mocks are crucial for validataion (*e.g.* Slepian et al. 2017). Moreover, as we show later in this paper, mocks present an additional advantage: they allow us to quantify the non-Gaussianity of the likelihood and more accurately estimate the true likelihood distribution.

In this paper, we we focus on two LSS analyses: the powerspectrum multipole (P_ℓ) analysis of B2017 and group multiplicity function (ζ) analysis of S2017. Throughout the paper we will make extensive use of the mock catalogs used in these analyses. In this section, we give a brief description of these mocks and how the observables used in the analysis — the powerspectrum multipole (P_ℓ) and group multiplicity function ($\zeta(N)$) — are calculated from them. Afterwards, we will describe how we compute the covariance matrix from the mocks and pre-process the mock observable data.

2.1. MultiDark-PATCHY Mock Catalog

In their powerspectrum multipole analysis, B2017 use the MultiDark-PATCHY mock catalogs from Kitaura et al. (2016). These mocks are generated using the PATCHY code (Kitaura et al. 2014, 2015). They rely on large-scale density fields generated using augmented Lagrangian Perturbation Theory (ALPT; Kitaura & Heß 2013) on a mesh, which they then populate with galaxies based on a combined non-linear deterministic and stochastic biases. The mocks from the PATCHY code are then calibrated to reproduce the galaxy clustering in the high-fidelity BigMultiDark N-body simulation (Rodríguez-Torres et al. 2016; Klypin et al. 2016). Afterwards, the galaxies are assigned stellar masses using the HADRON code (Zhao et al. 2015). and the SUGAR code (Rodríguez-Torres et al. 2016) is applied to combine different boxes, incorporate selection effects and masking to produce mock light-cone galaxy catalogs. The statistics of the resulting mocks are then compared to observations and the process is iterated to reach desired accuracy. We refer readers to Kitaura et al. (2016) for further details.

In total, Kitaura et al. (2016) generated a 12,228 mock light-cone galaxy catalogs for BOSS Data Release 12. In B2017, they use 2045 and 2048 for the northern galactic cap (NGC) and souther galactic cap (SGC) of the LOWZ+CMASS combined sample. B2017 excluded 3 mock realizations due to notable issues, which have been since been addressed. Therefore,

in our analysis we use all 2048 mocks for both the NGC and SGC of the LOWZ+CMASS combined sample.

2.2. Sinha et al. (2017) Mocks

The simulations used in the small-scale clustering analysis of Sinha et al. (2017) are from the Large Suite of Dark Matter Simulations project (LasDamas; McBride et al. 2009) designed to model galaxy samples from SDSS DR7. They use initial conditions derived from second order Lagrangian Perturbation Theory using the 2LTPIC code (Scoccimarro 1998; Crocce et al. 2006) and evolved them using the N-body GADGET-2 code (Springel 2005). Halos are then identified from the dark matter distribution outputs using the $\mathtt{ntropy - fofsv}$ code (Gardner et al. 2007), which uses a friend-of-friends algorithm (FoF; Davis et al. 1985) with a linking length of 0.2 times the mean inter-particle separation. S2017 uses two configurations of the LasDamas simulations. The Consuelo simulation contains 1400^3 dark matter particles with mass of $1.87 \times 10^9 \, h^{-1} M_\odot$ in a cubic volume of $420 \, h^{-1} Mpc$ per side evolved from $z_{\mathrm{init}} = 99$. The Carmen simulation contains 1120^3 dark matter particles with mass of $4.938 \times 10^{10} \, h^{-1} M_\odot$ in a cubic volume of $1000 \, h^{-1} Mpc$ per side evolved from $z_{\mathrm{init}} = 49$.

The FoF halo catalogs are then populated with galaxies using the 'Halo Occupation Distribution' (HOD) framework. The number, positions, and velocities of galaxies are described statistically by an HOD model. S2017 adopts the 'vanilla' HOD model of Zheng et al. (2007), where the mean number of central and satellite galaxies are described by the halo mass and five HOD parameters: $M_{\min}, \sigma_{\log M}, M_0, M_1,$ and α. Lastly, once the simulation boxes are populated with galaxies, observational systematic effects are imposed. The peculiar velocities of galaxies are used to impose redshift-space distortions. Galaxies that lie outside the redshift limits or sky footprint of the SDSS sample are removed. For further details regarding the mocks, we refer readers to S2017.

To calculate their covariance matrix, S2017 produced 200 independent mock catalogs from 50 simulations using a single set of HOD model parameters. To take advantage of the methods we later present (Sections 4.1 and 4.2), we require a large number of mocks. Our methods rely on using the mocks to sample high dimensional distributions, so incorporating more mocks improves their accuracy. We utilize an addition 99 sets of HOD parameters with 200 mocks each. These parameters are sampled from the MCMC chain used to produce the posterior in S2017. In total we use $20,000$ mocks.

2.3. Mock Observable $\mathbf{X}^{\mathrm{mock}}$ and Covariance Matrix $\mathbb{C}$

To get from the mock catalogs described above to the covariance matrices used in B2017 and S2017, the observables are measured for each mock in the *same* way as the observations. We briefly describe how $P_\ell(k)$ and $\zeta(N)$ and their covariance matrices are mea-

sured in B2017 and S2017. We then describe how we pre-process the mock observables for the methods we describe in the next sections.

To measure the powerspectrum multipoles of the BOSS DR12 galaxies and the MutliDark-PATCHY mocks (Section 2.1), B2017 uses a fast fourier transform (FFT) based anisotropic powerspectrum estimator based on Bianchi et al. (2015) and Scoccimarro (2015). This estimator estimates the monopole, quadrupole, and hexadecapole ($\ell = 0, 2,$ and 4) of the powerspectrum using FFTs of the overdensity field multipoles for a given survey geometry. For further details on the estimator we refer readers to B2017 Section 3. B2017 compute the powerspectrum over the range $k = 0.01 - 0.15 \, h \, \mathrm{Mpc}^{-1}$ for $\ell = 0,$ and 2 and $k = 0.01 - 0.10 \, h \, \mathrm{Mpc}^{-1}$. for $\ell = 4$. The powerspectrum multipoles are calculated in bins of $\Delta k = 0.01 \, h \, \mathrm{Mpc}^{-1}$.

From the $\vec{P}^{(n)} = \left[P_0^{(n)}(k), P_2^{(n)}(k), P_4^{(n)}(k) \right]$ of the MultiDark-PATCHY mocks, B2017 computes the (i,j) element of the covariance matrix of all multipoles as

$$\mathbb{C}_{i,j} = \frac{1}{N_{\mathrm{mock}} - 1} \sum_{n=1}^{N_{\mathrm{mock}}} \left[\vec{P}_i^{(n)} - \overline{P}_i \right] \times \left[\vec{P}_j^{(n)} - \overline{P}_j \right]. \tag{1}$$

$N_{\mathrm{mock}} = 2048$ is the number of mocks and $\overline{P}_i$ is the mean of the mock powerspectra: $\overline{P}_i = \frac{1}{N_{\mathrm{mock}}} \sum_{n=1}^{N_{\mathrm{mock}}} \vec{P}_i^{(n)}$. Since P_0 and P_2 each have 14 bins and P_4 has 9 bins, $\mathbb{C}$ is a 37×37 matrix. In this work, we compute the $P_\ell(k)$ using a similar FFT-based estimator of Hand et al. (2017) instead of the B2017 estimator. Our choice is based on computational convenience. A python implementation of the Hand et al. (2017) estimator is publicly available in the NBODYKIT package[3] (?). We confirm that the resulting $P_\ell(k)s$ and covariance matrices from the two estimators are consistent with one another.

Next, for the S2017 group multiplicity function analysis, they start with the Berlind et al. (2006) FoF algorithm to identify groups in the SDSS and mock data. S2017 adopts the Berlind et al. (2006) linking lengths in units of mean inter-galaxy separation: $b_\perp = 0.14$ and $b_\parallel = 0.75$. In comoving lengths, the linking lengths for the SDSS DR7 $M_r < -19$ sample correspond to $(r_\perp, r_\parallel) = (0.57, 3.05)h^{-1}$ Mpc. Once the groups are identified in the SDSS and mock data, $\zeta(N)$ is derived by calculating the comoving number density of groups in bins of richness N — the number of galaxies in the group. For the $M_r < 19$ SDSS sample, S2017 uses eight N bins: $(5 - 6), (7 - 9), (10 - 13), (14 - 19), (20 - 32), (33 - 52), (53 - 84), (85 - 220)$. For further details on the GMF calculation, we refer readers to S2017 Section 4.2. From the $\zeta^{(n)}(N)s$ of each mock, S2017 computes the (i,j) element of the covariance matrix as

$$\mathbb{C}_{i,j} = \frac{1}{N_{\mathrm{mock}} - 1} \sum_{n=1}^{N_{\mathrm{mock}}} \left[\zeta^{(n)}(N_i) - \bar{\zeta}(N_i) \right] \times \left[\zeta^{(n)}(N_j) - \bar{\zeta}(N_j) \right]. \tag{2}$$

In S2017, they compute the covariance matrix using 200 mocks generated using a single fiducial set of HOD parameters. As we describe in Section 2.2, in this paper we use 20,000

---

[3]http://nbodykit.readthedocs.io/en/latest/index.html

mocks from 100 different set of HOD parameters sampled from the MCMC chain. The GMF covariance matrix we use in this paper is computed with $N_{\mathrm{mock}} = 20,000$ mocks.

For the rest of the paper, in order to discuss the two separate analyses of B2017 and S2017 in a consistent manner, we define the matrix $\mathbf{D}^{\mathrm{mock}}$ of the mock observables (P_ℓ and ζ) as

$$\mathbf{D}^{\mathrm{mock}} = \left\{\mathbf{D}_n^{\mathrm{mock}}\right\} \qquad \text{where } \mathbf{D}_n^{\mathrm{mock}} \begin{cases} \vec{P}^{(n)} & \text{for B2017,} \\ \zeta^{(n)} & \text{for S2017.} \end{cases} \tag{3}$$

$\mathbf{D}^{\mathrm{mock}}$ has dimensions of 2048×37 and $20,000 \times 8$ for B2017 and S2017 respectively.

For the methods in Sections 4.1 and 4.2, the mock observable data ($\mathbf{D}^{\mathrm{mock}}$) need to be pre-processed. **why preprocess** This pre-processing involves two steps: mean-subtraction and whitening. For mean subtraction, the mean of the observable is subtracted from $\mathbf{D}^{\mathrm{mock}}$. Then $\mathbf{D}^{\mathrm{mock}} - \overline{\mathbf{D}}^{\mathrm{mock}}$ is whitened using a linear transformation to remove the Gaussian correlation between the bins of $\mathbf{D}^{\mathrm{mock}}$:

$$\mathbf{X}^{\mathrm{mock}} = L\left(\mathbf{D}^{\mathrm{mock}} - \bar{\mathbf{D}}^{\mathrm{mock}}\right). \tag{4}$$

The linear transformation is derived so that covariance matrix of the whitened data, $\mathbf{X}^{\mathrm{mock}}$, is the identity matrix $\mathbb{I}$. Such a whitening linear transformation can be derived in infinite ways. One way to derive the linear transformation is through the eigen-decomposition of the covariance matrix (*e.g.* Hartlap et al. 2009; Sellentin et al. 2017). We, alternatively, derive the linear transformation $\mathbf{L}$ using Choletsky decompositon of the inverse covariance matrix (Press et al. 1992): $\mathbb{C}^{-1} = \mathbf{L}\,\mathbf{L}^T$. **We confirm tha the different whitening algorithms, does not impact the results of the paper.** Now that we have the pre-processed data of the mock observables, we proceed in the next section to quantifying the non-Gaussianity of the P_ℓ and ζ likelihoods.

3. Quantifying the Likelihood non-Gaussianity

The standard approach to parameter inference in LSS studies neglects to account for likelihood non-Gaussianity. However, we are not the first to investigate likelihood non-Gaussianity in LSS analyses. Nearly two decades ago, Scoccimarro (2000) examined the likelihood non-Gaussianity for the powerspectrum and reduced bispectrum using mock catalogs of the IRAS redshift catalogs. More recently, Hartlap et al. (2009) and Sellentin et al. (2017) examined the non-Gaussianity of the cosmic shear correlation function likelihood using simulations of the Chandra Deep Field South and CFHTLenS, respectively.

While these works present different methods for identifying likelihood non-Gaussianity, they do not present a concrete way of quantifying it. Hartlap et al. (2009), for instance, identifies the non-Gaussianity of the cosmic shear likelihood by looking at the statistical

independence/dependence of PCA components of the mock observable. In Sellentin et al. (2017), they use the Mean Integrated Squared Error (MISE) as a distance metric between Gaussian random variables and the whitened mock observable data vector to characterize non-Gaussian correlations between elements of the data vector. These indirect measures of likelihood non-Gaussianity are challenging to interpret and extend more generally to LSS studies.

A more direct approach, however, can be taken to quantify the non-Gaussianity of the likelihood. We can calculate the divergence between the distribution of our observable, $p(x)$, and $q(x)$ a multivariate Gaussian described by the average of the mocks and the covariance matrix. The following are two of the most commonly used divergences: the Kullback-Leibler (KL) divergence

$$D_{KL}(p \parallel q) = \int p(x) \log \frac{p(x)}{q(x)} \, \mathrm{d}x \tag{5}$$

and the Rényi-α divergence

$$D_{R-\alpha}(p \parallel q) = \frac{1}{\alpha - 1} \log \int p^\alpha(x) \, q^{1-\alpha}(x) \, \mathrm{d}x. \tag{6}$$

In the limit as α approaches 1, the Rényi-α divergence is equivalent to the KL divergence.

Of course, in our case, we don't know $p(x)$ — i.e. the distribution of our observable. If we did, we would simply use that instead of bothering with the covariance matrix or this paper. We can, however, still estimate the divergence using nonparametric divergence estimators (Wang et al. 2009; Póczos et al. 2012; Krishnamurthy et al. 2014). These estimators allow us to estimate the divergence directly from samples $X_{1:n} = \{X_1, ... X_n\}$ and $Y_{1:m} = \{Y_1, ... Y_m\}$ drawn from p and q respectively: $\hat{D}_\alpha(X_{1:n} \parallel Y_{1:m})$. For instance, the estimator presented in Póczos et al. (2012) allows us to estimate the kernel function of the Rényi-α divergence,

$$D_\alpha(p \parallel q) = \int p^\alpha(x) q^{1-\alpha}(x) \, \mathrm{d}x. \tag{7}$$

using k^{th} nearest neighbor density estimators. Let $\rho_k(x)$ denote the Euclidean distance of the kth nearest neighbor of x in the sample $X_{1:n}$ and $\nu_k(x)$ denote the Euclidean distance of the kth nearest neighbor of x in the sample $Y_{1:m}$. Then

$$D_\alpha(p \parallel q) \approx \hat{D}_\alpha(X_{1:n} \parallel Y_{1:m}) = \frac{B_{k,\alpha}}{n} \left(\frac{n-1}{m} \right)^{1-\alpha} \sum_{i=1}^n \left(\frac{\rho_k^d(X_i)}{\nu_k^d(X_i)} \right)^{1-\alpha}, \tag{8}$$

where $B_{k,\alpha} = \frac{\Gamma(k)^2}{\Gamma(k-\alpha+1)\Gamma(k+\alpha-1)}$. This estimator, as Póczos et al. (2012) proves, is asymptotically unbias,

$$\lim_{n,m \to \infty} \mathbb{E}\left[\hat{D}_\alpha(X_{1:n} \parallel Y_{1:m}) \right] = D_\alpha(p \parallel q). \tag{9}$$

Plugging $\hat{D}_\alpha(X_{1:n} \parallel Y_{1:m})$ into Eq. 6, we get an estimator for the Rényi-α divergence. Wang et al. (2009) dervies a similar estimator for the KL divergence (Eq. 5).

These divergence estimates have been applied to Support Vector Machines and used extensively in the machine learning and astronomical literature with great success **elaborate a lot more**

- Compile papers that use this divergence, Ntampaka et al. (2015, 2016)

For more details on the non-parametric divergence estimators, we refer readers to Póczos et al. (2012) and Krishnamurthy et al. (2014).

With these estimators, we can now explicitly quantify the non-Gaussianity of the likelihood by computing the divergence between the likelihood distribution and the Gaussian pseudo-likelihood distribution: $D(p(x) \parallel \mathcal{N}(\overline{\mathbf{X}}^{\mathrm{mock}}, \mathbb{C}))$. We draw a reference sample $\mathbf{Y}^{\mathrm{ref}}$ from $\mathcal{N}(\overline{\mathbf{X}}^{\mathrm{mock}}, \mathbb{C})$ then since $\mathbf{X}^{\mathrm{mock}}$ is in principle sampled from $p(x)$, we can use the estimators to compute $\hat{D}(\mathbf{X}^{\mathrm{mock}} \parallel \mathcal{N})$. Similar to the experiments detailed in Póczos et al. (2012), we construct $\mathbf{Y}^{\mathrm{ref}}$ with a comparable sample size as $\mathbf{X}^{\mathrm{mock}}$: 2000 and 10,000 for the P_ℓ and ζ analyses respectively.

In Figure 1, we present the resulting Rényi-α (left) and KL (right) divergences ($\hat{D}_{R\alpha}$ and $\hat{D}_{KL}$; orange) for the B2017 P_ℓ (top) and S2017 ζ (bottom) analyses. As a reference for comparison, we also include in blue divergence estimates of the pseudo-likelihood onto itself, which we calculate as $\hat{D}(\mathbf{X}^{\mathrm{ref}} \parallel \mathbf{Y}^{\mathrm{ref}})$. $\mathbf{X}^{\mathrm{ref}}$ is a data vector with the same dimension as $\mathbf{X}^{\mathrm{mock}}$ sampled from the pseudo-likelihood $\mathcal{N}$. Since $\hat{D}$ are estimates, rather than the true divergence, we compute each of the estimates **100** times (resampling $\mathbf{Y}^{\mathrm{ref}}$ each time) and present their distribution in order to illustrate their uncertainty. Each panel of Figure 1 show significant discrepancy between the two distributions. This suggests that both the $P_\ell(k)$ and $\zeta(N)$ likelihoods are *significantly non-Gaussian*.

4. Estimating the Non-Gaussian Likelihood

In the previous section, we estimate the divergence between the P_ℓ and ζ likelihoods sampled by mocks and their respective Gaussian pseudo-likelihoods. These divergences identify and quantify the significant non-Gaussianity in the likelihoods of LSS studies. Our ultimate goal, however, is to quantify the impact of likelihod non-Gaussianity on the final cosmological parameter constrains and to develop more accurate methods for parameter inference in LSS. From the divergence estimates alone, it's not obvious how they propagate onto the final parameter constraints. Therefore in this section, we present two methods for more accurately estimating the non-Gaussian likelihoods of P_ℓ and ζ from the corresponding mocks. These methods provide a more accurate estmiate of the likelihood than the Gaussian pseudo-likelihood. Moreover, we will use them later to quantify the impact of likelihood non-Gaussianity on the B2017 and S2017 parameter constraints.
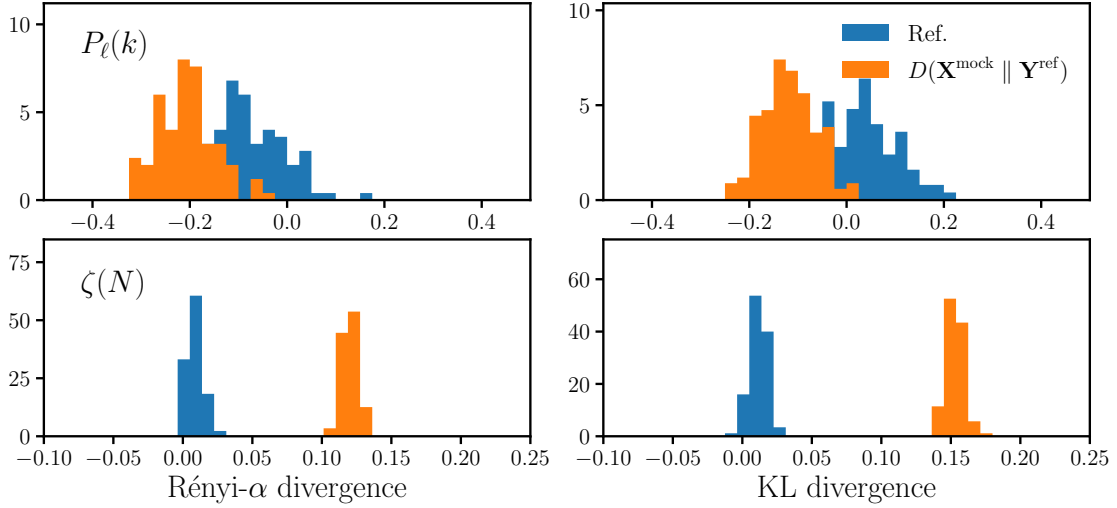
Fig. 1.— Rényi-α and KL divergence estimates ($\hat{D}_{R\alpha}$ and $\hat{D}_{KL}$; orange) between the likelihood distribution and the Gaussian pseudo-likelihood for the B2017 P_ℓ (top) and S2017 ζ (bottom) analyses. We include in blue, as reference, the divergence estimates of the pseudo-liklihood onto itself. $\hat{D}_{R\alpha}$ and $\hat{D}_{KL}$ are computed using the non-parametric k-NN estimator (Section 3) on the mock data $\mathbf{X}^{\mathrm{mock}}$ and a referece sample $\mathbf{Y}^{\mathrm{ref}}$ drawn from the pseudo-likelihood. We compute $\hat{D}_{R\alpha}$ and $\hat{D}_{KL}$ **100** times and plot their distribution in order to illustrate the uncertainty in the $\hat{D}$ estimator. The significant discrepancy between the two divergence distributions in each of the panels, identifies the *significant non-Gaussianity of the $P_\ell(k)$ and $\zeta(N)$ likelihoods.*

4.1. Gaussian Mixture Likelihood Estimation

When mock catalogs are used for parameter inference in LSS analyses, they essentialy serve as data points sampling the likelihood distribution. For the pseudo-likelihood, this distribution is assumed to have a Gaussian functional form. Hence, why we estimate the covariance matrix from mocks. However, the Gaussian functional form, or any functional form for that matter, is *not* necessary to estimate the likelihood distribution. Instead, the multidimensional likelihood distribution can be directly estimated from the set of mock catalogs using — for instance using Gaussian mixture density estimation (McLachlan & Peel 2000). **talk about how this is used extensively in ML** In astronomy, Gaussian mixture density estimation has been used for inferring the velocity distribution of stars from the Hipparcos satellite (Bovy et al. 2011), classifying galaxies in the Galaxy And Mass Assembly Survey (Taylor et al. 2015), and classifying pulsars (Lee et al. 2012; see also references in Kuhn & Feigelson 2017).

Gaussian mixutre density estimation is a "semi-parametric" method that uses a weighted sum of k Gaussian component densities, a Gaussian mixture model (hereafter GMM)

$$p(x; \boldsymbol{\theta}) = \sum_{i=1}^{k} \pi_i \, \mathcal{N}(x; \boldsymbol{\theta}_i), \qquad (10)$$

to estimate the density. The component weights (π_i; also known as mixing weights) and the component parameters $\boldsymbol{\theta}_i$ are free parameters of the mixture model. Given some data set $\mathbf{X}_N = \{\mathbf{x}_1, ..., \mathbf{x}_N\}$, these free GMM parameters are, most popularly, estimated through an expectation-maximization algorithm (EM; Dempster et al. 1977; Neal & Hinton 1998). The EM algorithm begins by randomly assigning $\boldsymbol{\theta}_i^0$ to the k Gaussian components. The algorithm then iterates between two steps. In the first step, the algorithm computes for each data point, $\mathbf{x}_n$, a probability of being generated by each component of the model. These probabilities can be thought of as weighted assignments of the points to the components. Next, given the $\mathbf{x}_n$ assignment to the components, $\boldsymbol{\theta}_i^t$ of each component are updated to $\boldsymbol{\theta}_i^{t+1}$ to maximize the likelihood of the assigned points. At this point, π_i can also be updated by summing up the assignment weights and normalizing it by the total number of data points, N. This entire process is repeated until convergence — *i.e.* when the log-likelihood of given the mixture model log $p(\mathbf{X}_N; \boldsymbol{\theta}^t)$ converges. The EM algorithm is guaranteed to converges to a local maximum of the likelihood (Wu 1983).

In practice, instead of arbitrarily assigning the initial condition, $\boldsymbol{\theta}_i^0$ is derived from a k-means clustering algorithm (Lloyd 1982). Without going into details, the k-means algorithm clusters the data $\mathbf{X}_N$ into k clusters, each described by the mean (or centroid) μ_i of the samples in the cluster. The algorithm then iteratively chooses centroids that minimize the average squared distance between points in the same cluster. For our GMMs, we set the initialize the EM algorithm using the k-means++ algorithm of Arthur & Vassilvitskii (2007).

In Figure 2, we illustrate Gaussian mixture density estimation in action. We use GMMs with $k = 1$ (top), 3 (middle), and 10 (bottom) components to estimate the distribution of one dimensional data (blue) drawn from three separate Gaussia distributions. The GMM outputs of the EM algorithm are plotted in red with dotted black lines representing each of their components.

So far in our description of GMMs, we have kept the number of componenets k fixed. However, k is a free parameter and selecting it is a crucial step in Gaussian mixture density estimation. With too many components the model may overfit the data; with too few components, the model may not be flexible enough to approximate the true underlying distribution. In order to address this model selection problem of selecting k, we make use of the Bayesian Information Criterion (BIC; Schwarz 1978). BIC has been widely used for determining the number of components in mixture modeling (*e.g.* Leroux 1992; Roeder & Wasserman 1997; Fraley & Raftery 1998; Steele & Raftery 2010) and for model selection in general in astronomy (*e.g.* Liddle 2007; Broderick et al. 2011; Wilkinson et al. 2015; Vakili & Hahn 2016). According to BIC, models with higher likelihood are preferred; however, to address the concern of overfitting, BIC introduces a *penalty* term for the number of parameters in the model:

$$\mathrm{BIC} = -2 \ln \mathcal{L} + N_{\mathrm{par}} \ln N_{\mathrm{data}}. \tag{11}$$

We select k based on the number of components in the model with the lowest BIC. Of the three panels in Figure 2, the GMM model with $k = 3$ components has the lowest BIC and therefore would be selected. At least in this example, the choice of $k = 3$ is obviously justified. The $k = 1$ GMM is definitely not flexible enough to characterize the underlying distribution and the $k = 10$ GMM clearly overfits the distribution.

With Gaussian mixture density estimation we can directly estimate the likelihood distribution using the mock catalogs. We first fit GMMs with ks < 30 components to the whitened mock data $\mathbf{X}^{\mathrm{mock}}$ using the EM algorithm for each model. For each of the coverged GMMs, we calculate the BIC. Afterwards we select the model with the lowest BIC as the best density estimate of the likelihood distribution: $\hat{p}_{\mathrm{GMM}}(x)$. The selected density estimate can then be used to calculate the likelihood and quantify the impact of likelihood non-Gaussianity on the parameter constraints of B2017 and S2017. But before we do that, we have to confirm whether $\hat{p}_{\mathrm{GMM}}$ is in fact a better estimate of the likelihood over the Gaussian pseudo-likelihood. To do this, we return to the divergence estimates of Section 3.

To estimate the divergence between our Gaussian mixture density estimate, $\hat{p}_{\mathrm{GMM}}$, and the likelihood distribution, we take the same approach as our $\hat{D}$ calculation in Section 3. Instead of $\mathbf{Y}^{\mathrm{ref}}$ drawn from the pseudo-likelihood, we draw samples from $\hat{p}_{\mathrm{GMM}}(x)$ with the same dimensions. Then we calculate k-NN Rényi-α and KL divergence estimates between this sample and $\mathbf{X}^{\mathrm{mock}}$. As we did in Figure 1, we repeat this process 100 times, resampling $\hat{p}_{\mathrm{GMM}}$ each time, in order get a distribution of divergence estimates that reflects the scatter in
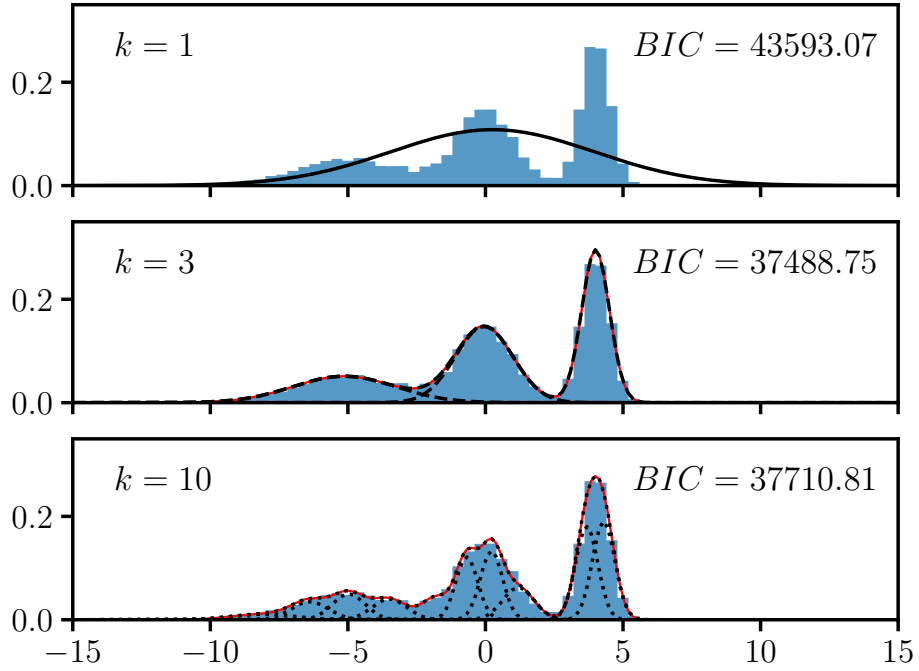
Fig. 2.— A pedagogical illustration of Gaussian mixture density estimation. We use GMMs with $k = 1$ (top), 3 (middle), 10 (bottom) components to estimate the distribution of data (blue) drawn from three Gaussian distributions. The GMM outputs of the EM algorithm are plotted in red with **dotted lines** representing each of their components (Section 4.1). We also include the BIC of the GMMs, which we use to select the number of components k. Of the three panels, $k = 3$ has the lowest BIC and therefore best represents the data according to our selection scheme.

the estimator. In Figure 3, we present the resulting distribution of divergences between $\hat{p}_{\mathrm{GMM}}$ and the likelihood distribution in **green** for the $P_\ell(k)$ (top) and $\zeta(N)$ (bottom) analyses. For comparison, we include the distributions from Figure 1.

For the $\zeta(N)$ analysis of S2017, our Gaussian mixture density estimate significantly improves the divergence discrepancy compared to the pseudo-likelihood. In other words, *our Gaussian mixture density estimate is a significant better estimate of the ζ likelihood distribution than the pseudo-likelihood.* On the other hand, our Gaussian mixture density estimate for the $P_\ell(k)$ analysis of B2017 does not significantly improve the divergence discrepancy. This difference in the performance of Gaussian mixture density estimation is not surprising. One would expect a direct density estimation to be more effective for the S2017 case, where we estimate an 8-dimensional distribution with $N_{\mathrm{mock}} = 20,000$ samples, compared to the B2017 case where we estimate a 37-dimensional distribution with only $N_{\mathrm{mock}} = 2048$ samples. Given the unconvincing accuracy of the Gaussian mixture density estimate of the P_ℓ likelihood, in the next section we present an alterative method for estimating the non-Gaussian likelihood.

4.2. Independent Component Analysis

Gaussian mixture density estimation fails to accurately estimate the 37-dimensional P_ℓ likelihood distribution of B2017. Rather than estimating the likelihood distribution directly, if we can transform the observable $\mathbf{x}$ (*e.g.* P_ℓ) into statistically independent components $\mathbf{x}^{\mathrm{IC}}$ the problem becomes considerably simpler. Since $\mathbf{x}^{\mathrm{IC}}$ is statistically independent the likelihood distribution becomes

$$p(x) = \prod_{n=1}^{N_{\mathrm{bin}}} p_{x_n^{\mathrm{IC}}}(x) \tag{12}$$

where N_{bin} is the number of bins in the observable. For the B2017 case, this reduces the problem of estimating a 37 dimensional distribution with 2048 samples to a problem of estimating 37 one dimensional distributions with 2048 samples each. The challenge, however, is in finding the transformation $\mathbf{M}$.

Efforts in the past have attempted to tackle this sort of high-dimensional problem (*e.g.* Scoccimarro 2000; Eisenstein & Zaldarriaga 2001; Gaztañaga & Scoccimarro 2005; Norberg et al. 2009; Sinha et al. 2017). They typically use singular value decomposition or principal component analysis (PCA; Press et al. 1992). For a Gaussian likelihood, the PCA components of it are statistically independent. However, when the likelihood is *not* Gaussian, the PCA components are uncorrelated but *not necessarily statistically independent* (Hartlap et al. 2009). Since the P_ℓ and ζ likelihoods are non-Gaussian, we cannot use PCA. Instead, we follow Hartlap et al. (2009) and use Independent Component Analysis (ICA Hérault & Ans 1984; Comon 1994; Hyvärinen & Oja 2000; Hyvarinen 2001).
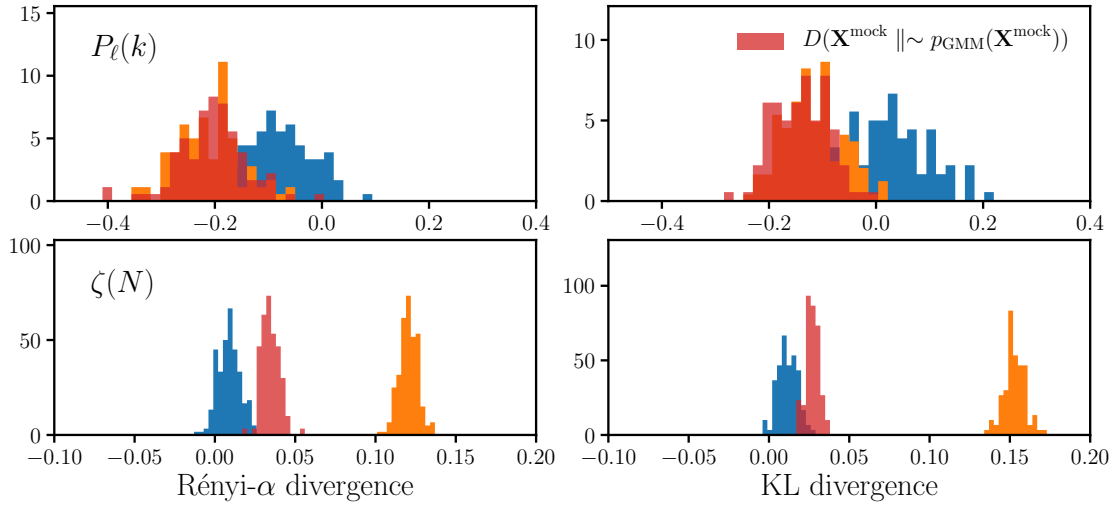
Fig. 3.— Rényi-α and KL divergence estimates ($\hat{D}_{R\alpha}$ and $\hat{D}_{KL}$; **green**) between the likelihood distribution and the Section 4.1 GMM likelihood estimate for the B2017 P_ℓ (top) and S2017 ζ (bottom) analyses. We include the divergence estimates from Figure 1 for comparison. The Gaussian mixture likelihood does not significantly improve the discrepancy in divergence for the P_ℓ analysis. This is due to the high-dimensionality (37 dimensions) of the P_ℓ likelihood. However, for the ζ analysis, *our Gaussian mixture likelihood estimate is a significantly better estimate of the likelihood than the pseudo-likelihood.*

In order to find the transformation of $\mathbf{x}$ to $\mathbf{x}^{\mathrm{IC}}$ we first assume that $\mathbf{x}$ is generated by some linear transformation $\mathbf{x} = \mathbf{M}\,\mathbf{x}^{\mathrm{IC}}$. The goal of ICA is to invert this problem, $\mathbf{y} = \mathbf{W}\,\mathbf{x}$, and find $\mathbf{W}$ and $\mathbf{y}$ that best estimate $\mathbf{y} \approx \mathbf{x}^{\mathrm{IC}}$. The basic premise of ICA is simple, maximizing non-Gaussianity maximizes the statistical independence. Consider a single component of $\mathbf{y}$:

$$\mathbf{y}_n = \mathbf{w}_n^t\,\mathbf{x} = \mathbf{w}_n^t\,\mathbf{M}\,\mathbf{x}^{\mathrm{IC}} \tag{13}$$

where $\mathbf{w}_n^t$ is the nth row of $\mathbf{W}$. Since $\mathbf{y}_n$ is a linear combination of the independent components $\mathbf{x}^{\mathrm{IC}}$, due to the Central Limit Theorem $\mathbf{y}_n$ is necessarily more Gaussian than any of the components *unless* $\mathbf{y}_n$ is equal to one of the $\mathbf{x}^{\mathrm{IC}}$ components. In other words, we can achieve $\mathbf{y} \approx \mathbf{x}^{\mathrm{IC}}$ by finding $\mathbf{W}$ that maximizes the non-Gaussianity of $\mathbf{y}$. For a more rigorous justification of ICA we refer readers to Hyvarinen (2001). In practice, non-Gaussianity is commonly measured using differential entropy — "negentropy". For $\mathbf{y}_n$ with density function p_{y_n} the entropy is defined as

$$H_{y_n} = -\int p_{y_n}(y)\,\log p_{y_n}(y)\,\mathrm{d}y. \tag{14}$$

Since the Gaussian distribution has the largest entropy among all distributions with a given variance, the negentropy can be defined as,

$$J_{y_n} = H_{y_n^{\mathrm{Gauss}}} - H_{y_n}. \tag{15}$$

Finding the statistically independent components is now a matter of finding the $\mathbf{W}$ that maximizes $\sum_n J_{\mathbf{y_n}}$ — the negentropy of $\mathbf{y}$. In this paper, we make use of the `FastICA` fixed-point iteration algorithm (Hyvarinen 1999). The algorithm starts with randomly selected $\mathbf{w}_n s$, then it uses approximations of negentropy from Hyvärinen (1998) and Newton's method to iteratively solve for $\mathbf{W}$ that maximizes negentropy. For details on the `FastICA` algorithm, we refer readers to Hyvarinen (1999).

Performing ICA on the whitened observable data $\mathbf{X}^{\mathrm{mock}}$, we derive the matrix $\mathbf{W}$ that transforms $\mathbf{X}^{\mathrm{mock}}$ into N_{bin} approximately independent components:

$$\mathbf{X}^{\mathrm{ICA}} = \mathbf{W}\,\mathbf{X}^{\mathrm{mock}} = \{\mathbf{X}_1^{\mathrm{ICA}}, ..., \mathbf{X}_{N_{\mathrm{bin}}}^{\mathrm{ICA}}\}. \tag{16}$$

From these statistically independent components and Eq. 12, we can estimate the likelihood distribution. $p_{x_n^{\mathrm{IC}}}(x)$, from Eq. 12, is the 1-dimensional distribution function of the nth ICA component. This distribution is sampled by $\mathbf{X}_n^{\mathrm{ICA}}$, the transformed mock data. That means $\mathbf{X}_n^{\mathrm{ICA}}$ can be used to estimate $p_{x_n^{\mathrm{ICA}}}$ using a method like kernel density estimation (KDE; *e.g.* Hastie et al. 2009; Feigelson & Babu 2012). With KDE, the density estimate, $\hat{p}_{x_n^{\mathrm{ICA}}}$, is constructed by smoothing the empirical distribution of the ICA componenet x_n^{ICA} using a smooth kernel:

$$\hat{p}_{x_n^{\mathrm{ICA}}}(x) = \frac{1}{N_{\mathrm{mock}}b} \sum_{j=1}^{N_{\mathrm{mock}}} K\left(\frac{x - \mathrm{X}_n^{(j),\mathrm{ICA}}}{b}\right). \tag{17}$$

b is the bandwidth and K is the kernel function. Following the choices of Hartlap et al. (2009), we use a Gaussian distribution for K and the "rule of thumb" bandwidth (also known as Scott's rule; Scott 1992; Davison 2008) for b. Combining all $N_{\rm bin}$ $\hat{p}_{x_n^{\rm ICA}}$ estimates into Eq. 12, we can estimate the likelihood distribution

$$p(x) \approx \prod_{n=1}^{N_{\rm bin}} \hat{p}_{x_n^{\rm ICA}}(x) \tag{18}$$

We again test whether the likelihood estimate from ICA is actually a better estimate of the likelihood distribution than the Gaussian pseudo-likelihood. Following the same procedure as we did for the Gaussian mixture likelihood in Section 4.1, we calculate the divergence between our ICA likelihood, $\prod \hat{p}_{x_n^{\rm ICA}}(x)$, and the likelihood distribution, $p(x)$. We draw a sample from $\prod \hat{p}_{x_n^{\rm ICA}}$ with the same dimensions as $\mathbf{Y}^{\rm ref}$ (Section 3), apply the mixing matrix (undoing the ICA transformation), and then calculate the k-NN Rényi-α and KL divergence estimates between the sample and $\mathbf{X}^{\rm mock}$. We repeat these steps **100** times to get the distribution of estimates that reflects the scatter in the estimator. In Figure 4, we present the resulting distribution of $\hat{D}\left(\mathbf{X}^{\rm mock} \,\|\sim \prod \hat{p}_{x_n^{\rm ICA}}\right)$ in **green** for the $P_\ell(k)$ (top) and $\zeta(N)$ (bottom) analyses. For comparison, we include the distributions from Figure 1.

For *both* B2017 and S2017, our ICA likelihood significantly improves the divergence discrepancy compared to the pseudo-likelihood. For S2017, however, the ICA likelihood proves to be a less accurate estimate than the Gaussian mixture likelihood in Section 4.1. More importantly, for B2017, where the Gaussian mixture likelihood did not improve upon the pseudo-likelihood, the ICA method provides a significantly more accurate likelihood estimate. This demonstrates that the ICA method is an alterative to the more direct Gaussian mixture method. Furthermore, the effectiveness of the ICA method in estimating higher dimensional likelihoods with fewer samples (mocks) is particularly appealing for LSS, since analyses continue to increase the size of their observable data vector. However, as the divergence estimation framework we present makes it easy to test the accuracy of different methods, a hard choice is not necessary and multiple methods can easily be tested to construct the best estimate of the likelihood distribution for each specific analysis. In the following sections, based on the performances of the GMM and ICA methods, we use the ICA method for the B2017 analysis and the GMM method for the S2017 analysis.

5. Impact on Parameter Inference

To derive the posterior distribution of their model parameters, both B2017 and S2017 use the standard Monte Carlo Markov Chain (MCMC) approach with the Gaussian pseduo-likelihood. The B2017 analysis contains 11 parameters,

$$\left\{f\sigma_8,\ \alpha_\parallel,\ \alpha_\perp,\ b_1^{\rm NGC}\sigma_8,\ b_1^{\rm SGC}\sigma_8,\ b_2^{\rm NGC}\sigma_8,\ b_2^{\rm SGC}\sigma_8,\ \sigma_v^{\rm NGC},\ \sigma_v^{\rm SGC},\ N^{\rm NGC},\ {\rm and}\ N^{\rm SGC}\right\},$$
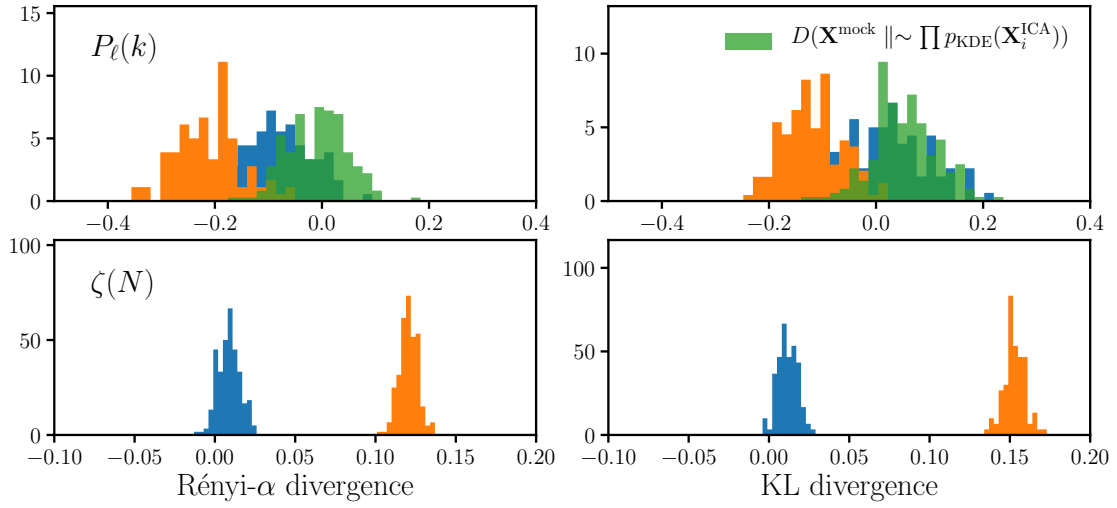
Fig. 4.— Rényi-α and KL divergence estimates ($\hat{D}_{R\alpha}$ and $\hat{D}_{KL}$; **green**) between the likelihood distribution and the Section 4.2 ICA likelihood estimate for the B2017 P_ℓ (top) and S2017 ζ (bottom) analyses. We include the divergence estimates from Figure 1 for comparison. The ICA likelihood significantly improves the divergence discrpancy for both the P_ℓ and ζ analyses. For ζ, the improvement of the ICA likelihood over the pseudo-likelihood is more modest than our GMM estimate from Section 4.1. However, for P_ℓ, where the GMM method struggled, our ICA likelihood provides a significant improvement.

while the S2017 analysis contains 5 parameters,

$$\left\{ \log\ M_{\mathrm{min}},\ \sigma_{\log\ M},\ \log\ M_0,\ \log\ M_1,\ \text{and}\ \alpha \right\}.$$

Using the improved likelihood estimates from the Sections 4.1 and 4.2, we can measure the impact of likelihood non-Gaussianity on the posterior distributions of these parameters. The most straightforward approach to do this would be to use the likelihood estimates to compute MCMC samples from scratch. While this is relatively doable for the B2017 analysis, for S2017 this is *significantly* more involved. Rather than a perturbation theory based model from B2017, the S2017 model is a forward model, same as their mocks (Section 2.2). Re-running the MCMC samples would involve evaluating their computational intensive forward model $> 10^5$ times.

Without having to re-run the MCMC chains, we instead use importance sampling to derive the new posteriors from the original chains (see Wasserman 2004, for details on importance sampling). The *target* distribution we want is the new posterior. To sample this distribution, we use the original posterior as the *proposal* distribution with the ratio of our likelihood estimates over the pseudo-likelihood as *importance weights*. If we let $P(\mathbf{x}|\boldsymbol{\theta})$ be the original pseudo-likelihood and $P'(\mathbf{x}|\boldsymbol{\theta})$ be our "new" likelihood, then the new marginal likelihood can be calculated through importance sampling:

$$P'(\mathbf{x}|\theta_1) = \int P'(\mathbf{x}|\boldsymbol{\theta})\,\mathrm{d}\theta_2...\mathrm{d}\theta_m = \int \frac{P'(\mathbf{x}|\boldsymbol{\theta})}{P(\mathbf{x}|\boldsymbol{\theta})}\,P(\mathbf{x}|\boldsymbol{\theta})\,\mathrm{d}\theta_2...\mathrm{d}\theta_m \tag{19}$$

Through Monte Carlo integration, this becomes

$$P'(\mathbf{x}|\theta_1) \approx \sum_{\boldsymbol{\theta}^{(i)}\in S} \frac{P'(\mathbf{x}|\boldsymbol{\theta}^{(i)})}{P(\mathbf{x}|\boldsymbol{\theta}^{(i)})}. \tag{20}$$

where S is the sample drawn from $P(\mathbf{x}|\boldsymbol{\theta})$. In our case S is just the original MCMC chain. The only calculation required is the importance weights in Eq. 20, $P'(\mathbf{x}|\boldsymbol{\theta}^{(i)})/P(\mathbf{x}|\boldsymbol{\theta}^{(i)})$ for each sample $\boldsymbol{\theta}^{(i)}$ of the original MCMC chain. To derive the importance sampled posterior distributions using the non-Gaussian likelihood estimates from this paper, $P(\mathbf{x}|\boldsymbol{\theta}^{(i)})$ is the pseudo-likelihood and $P'(\mathbf{x}|\boldsymbol{\theta}^{(i)})$ is the ICA likelihood for B2017 and the GMM likelihood S2017.

We present in Figure 5 the resulting posterior distributions using the non-Gaussian ICA likelihood for the $\left\{ f\sigma_8,\ \alpha_\|,\ \alpha_\perp,\ b_1^{\mathrm{NGC}}\sigma_8,\ b_1^{\mathrm{SGC}}\sigma_8,\ b_2^{\mathrm{NGC}}\sigma_8,\ b_2^{\mathrm{SGC}}\sigma_8, \right\}$ parameters in the B2017 P_ℓ analysis (orange). We include the original B2017 posterior distributions for comparison in blue. On the bottom of each panel, we include box plots marking the confidence interals of the updated and original posteriors. The boxes and "whiskers" repesent the 68% and 95% confidence intervals, respectively. We also list the median and 68% confidence intervals of the posteriors in Table 1. Overall, likelihood non-Gaussianity does *not* have a significant impact
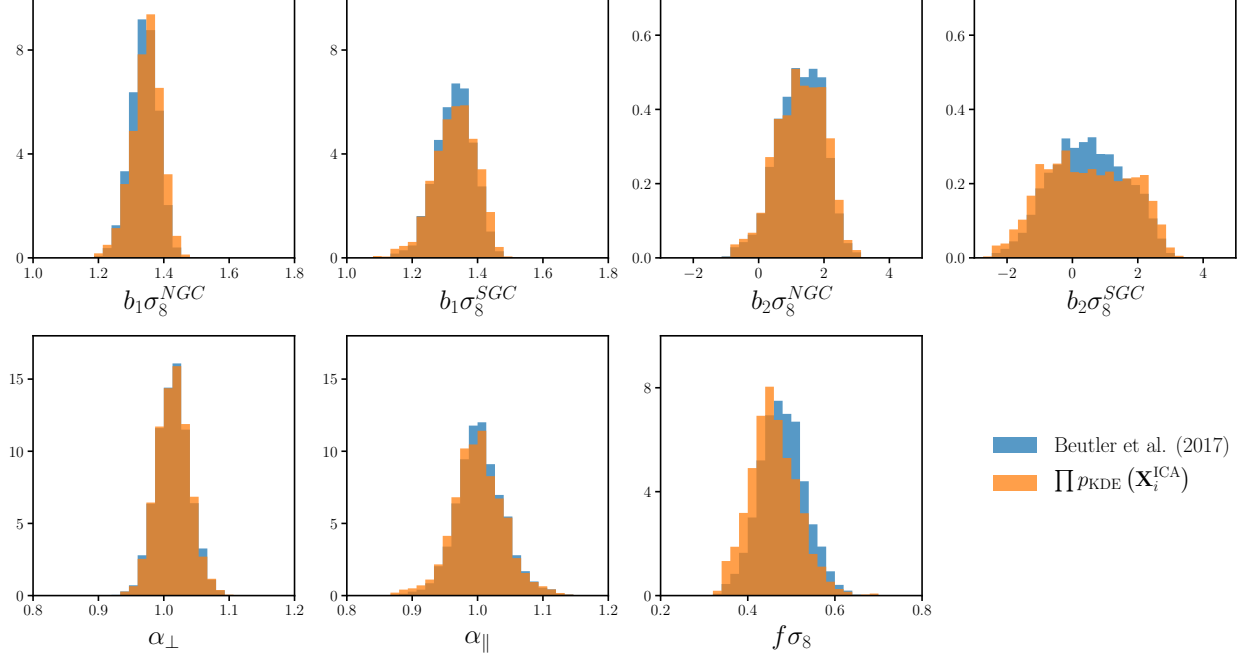
Fig. 5.— The posterior distribution for $\left\{ f\sigma_8,\ \alpha_\parallel,\ \alpha_\perp,\ b_1^{\mathrm{NGC}}\sigma_8,\ b_1^{\mathrm{SGC}}\sigma_8,\ b_2^{\mathrm{NGC}}\sigma_8,\ b_2^{\mathrm{SGC}}\sigma_8, \right\}$ in the B2017 P_ℓ analysis using the non-Gaussian ICA likelihood (orange). We include in blue the original B2017 posteriors for comparison. On the bottom of each panel we include box plots that mark the 68% and 95% confidence intervals of the posterior. The discrepancy between the posteriors is most evident for the parameters $f\sigma_8$ and and $b_2\sigma_8$. Overall, however, likelihood non-Gaussianity does *not* have a siginificant impact on the parameter constraints of the P_ℓ analysis.

on the parameter constraints of the P_ℓ analysis. $f\sigma_8$ and $b_2\sigma_8$ are the main parameters with noticeable change in their posteriors. **put the actual numbers**

Focusing on the main cosmological parameters $f\sigma_8$, $\alpha_\parallel$, and $\alpha_\perp$, we present their joint posterior distributions in Figure 6. The contours mark the 68% and 95% confidence intervals of the posteriors. The shift in the $f\sigma_8$ distribution is reflected in the $(f\sigma_8, \alpha_\parallel)$ and $(\alpha_\perp, f\sigma_8)$ contours (left and middle panels respectively). Meanwhile, the $(\alpha_\parallel, \alpha_\perp)$ distribution (right) show nearly no change from the non-Gaussian likelihood. These joint posteriors corroborate our conclusion from Figure 5.

Next in Figure 7, we present the posterior distributions calcuated using the non-Gaussian GMM likelihood for the HOD parameters in the S2017 ζ analysis (orange). We include the posteriors calculated using the pseudo-likelihood for comparison in blue. The box plots on the bottom of each plot mark the 68% and 95% confidence intervals of the posteriors. We also list the median and 68% confidence intervals in Table 1. In dotted lines, we plot the original S2017 posteriors, which differ from the blue distribution. This difference is caused by the difference in the covariance matrix we use in the pseudo-likelihood (see Section 2.3). The difference, however, is negiligible.

Likelihood non-Gaussianity significantly impacts the posterior distribution of all the HOD parameters except $\log M_0$. **put in details once the numbers out** The impact of likelihood non-Gaussianity is further emphasized in the joint posterior distributions of Figure 8. The $(\log M_{\min}, \sigma_{\log M})$ and $(\log M_{\min}, \alpha)$ contours are both shifted and broadened.

6. Discussion

- Will it matter for future surveys?

- Likelihood free inference (cite justin's paper)

Table 1: Impact of likelihood non-Gaussianity on the posterior parameter constraints of B2017 and S2017

B2017 P_ℓ analysis						
$f\sigma_8$	$\alpha_\parallel$	$\alpha_\perp$	$b_1^{\mathrm{NGC}}\sigma_8$	$b_1^{\mathrm{SGC}}\sigma_8$	$b_2^{\mathrm{NGC}}\sigma_8$	$b_2^{\mathrm{SGC}}\sigma_8$
B2017						
0.478	$\alpha_\parallel$	$\alpha_\perp$	$b_1^{\mathrm{NGC}}\sigma_8$	$b_1^{\mathrm{SGC}}\sigma_8$	$b_2^{\mathrm{NGC}}\sigma_8$	$b_2^{\mathrm{SGC}}\sigma_8$
non-Gaussian $\mathcal{L}_{\mathrm{ICA}}$						
0.478	$\alpha_\parallel$	$\alpha_\perp$	$b_1^{\mathrm{NGC}}\sigma_8$	$b_1^{\mathrm{SGC}}\sigma_8$	$b_2^{\mathrm{NGC}}\sigma_8$	$b_2^{\mathrm{SGC}}\sigma_8$

7.   Summary

Acknowledgements

It's a pleasure to thank Simone Ferraro, David W. Hogg, Emmaneul Schaan, Roman Scoccimarro Zachary Slepian

REFERENCES

Alam, S., Ata, M., Bailey, S., et al. 2017, Monthly Notices of the Royal Astronomical Society, 470, 2617

Arthur, D., & Vassilvitskii, S. 2007, in Proceedings of the Eighteenth Annual ACM-SIAM Symposium on Discrete Algorithms, SODA '07 (Philadelphia, PA, USA: Society for Industrial and Applied Mathematics), 1027

Berlind, A. A., Frieman, J., Weinberg, D. H., et al. 2006, The Astrophysical Journal Supplement Series, 167, 1

Beutler, F., Seo, H.-J., Saito, S., et al. 2017, Monthly Notices of the Royal Astronomical Society, 466, 2242

Bianchi, D., Gil-Marín, H., Ruggeri, R., & Percival, W. J. 2015, Monthly Notices of the Royal Astronomical Society, 453, L11

Bovy, J., Hogg, D. W., & Roweis, S. T. 2011, The Annals of Applied Statistics, 5, 1657

Broderick, A. E., Fish, V. L., Doeleman, S. S., & Loeb, A. 2011, The Astrophysical Journal, 735, 110

Comon, P. 1994, Signal Processing, 36, 287

Crocce, M., Pueblas, S., & Scoccimarro, R. 2006, Monthly Notices of the Royal Astronomical Society, 373, 369

Davis, M., Efstathiou, G., Frenk, C. S., & White, S. D. M. 1985, The Astrophysical Journal, 292, 371

Davison, A. C. 2008, Statistical Models (Cambridge Series in Statistical and Probabilistic Mathematics) (Cambridge University Press)

Dempster, A. P., Laird, N. M., & Rubin, D. B. 1977, Journal of the Royal Statistical Society. Series B (Methodological), 39, 1

Eisenstein, D. J., & Zaldarriaga, M. 2001, The Astrophysical Journal, 546, 2

Feigelson, E. D., & Babu, G. J. 2012, Modern Statistical Methods for Astronomy

Fraley, C., & Raftery, A. E. 1998, The Computer Journal, 41, 578

Gardner, J. P., Connolly, A., & McBride, C. 2007, in Astronomical Data Analysis Software and Systems XVI, Vol. 376, 69

Gaztañaga, E., & Scoccimarro, R. 2005, Monthly Notices of the Royal Astronomical Society, 361, 824

Grieb, J. N., Sánchez, A. G., Salazar-Albornoz, S., et al. 2017, Monthly Notices of the

Royal Astronomical Society, 467, 2085

Guo, H., Zehavi, I., & Zheng, Z. 2012, The Astrophysical Journal, 756, 127

Hahn, C., Scoccimarro, R., Blanton, M. R., Tinker, J. L., & Rodríguez-Torres, S. A. 2017, Monthly Notices of the Royal Astronomical Society, 467, 1940

Hand, N., Li, Y., Slepian, Z., & Seljak, U. 2017, Journal of Cosmology and Astro-Particle Physics, 07, 002

Hartlap, J., Schrabback, T., Simon, P., & Schneider, P. 2009, Astronomy and Astrophysics, 504, 689

Hastie, T., Tibshirani, R., & Friedman, J. 2009, The Elements of Statistical Learning: Data Mining, Inference, and Prediction, Second Edition (Springer Series in Statistics) (Springer)

Hérault, J., & Ans, B. 1984, Comptes Rendus de l'Académie des Sciences Paris, Série III, Life Sciences, 299, 525

Hyvärinen, A. 1998, in Advances in Neural Information Processing Systems 10, ed. M. I. Jordan, M. J. Kearns, & S. A. Solla (MIT Press), 273

Hyvarinen, A. 1999, IEEE Transactions on Neural Networks, 10, 626

—. 2001, Independent Component Analysis (New York: J. Wiley)

Hyvärinen, A., & Oja, E. 2000, Neural Networks: The Official Journal of the International Neural Network Society, 13, 411

Kazin, E. A., Koda, J., Blake, C., et al. 2014, Monthly Notices of the Royal Astronomical Society, 441, 3524

Kitaura, F.-S., Gil-Marín, H., Scóccola, C. G., et al. 2015, Monthly Notices of the Royal Astronomical Society, 450, 1836

Kitaura, F.-S., & Heß, S. 2013, Monthly Notices of the Royal Astronomical Society, 435, L78

Kitaura, F.-S., Yepes, G., & Prada, F. 2014, Monthly Notices of the Royal Astronomical Society, 439, L21

Kitaura, F.-S., Rodríguez-Torres, S., Chuang, C.-H., et al. 2016, Monthly Notices of the Royal Astronomical Society, 456, 4156

Klypin, A., Yepes, G., Gottlöber, S., Prada, F., & Heß, S. 2016, Monthly Notices of the Royal Astronomical Society, 457, 4340

Krishnamurthy, A., Kandasamy, K., Poczos, B., & Wasserman, L. 2014, arXiv:1402.2966 [math, stat], arXiv:1402.2966 [math, stat]

Kuhn, M. A., & Feigelson, E. D. 2017, arXiv:1711.11101 [astro-ph, stat], arXiv:1711.11101 [astro-ph, stat]

Lee, K. J., Guillemot, L., Yue, Y. L., Kramer, M., & Champion, D. J. 2012, Monthly Notices of the Royal Astronomical Society, 424, 2832

Leroux, B. G. 1992, The Annals of Statistics, 20, 1350

Liddle, A. R. 2007, Monthly Notices of the Royal Astronomical Society, 377, L74

Lloyd, S. 1982, IEEE Transactions on Information Theory, 28, 129

McBride, C., Berlind, A., Scoccimarro, R., et al. 2009, in Bulletin of the American
        Astronomical Society, Vol. 213, 425.06

McLachlan, G., & Peel, D. 2000, Finite Mixture Models (Wiley-Interscience)

Mohammed, I., Seljak, U., & Vlah, Z. 2017, Monthly Notices of the Royal Astronomical
        Society, 466, 780

Neal, R. M., & Hinton, G. E. 1998, in Learning in Graphical Models, NATO ASI Series
        (Springer, Dordrecht), 355

Norberg, P., Baugh, C. M., Gaztañaga, E., & Croton, D. J. 2009, Monthly Notices of the
        Royal Astronomical Society, 396, 19

Ntampaka, M., Trac, H., Sutherland, D. J., et al. 2015, The Astrophysical Journal, 803, 50

—. 2016, The Astrophysical Journal, 831, 135

Parkinson, D., Riemer-Sørensen, S., Blake, C., et al. 2012, Physical Review D, 86, 103518

Pinol, L., Cahn, R. N., Hand, N., Seljak, U., & White, M. 2017, Journal of Cosmology and
        Astroparticle Physics, 2017, 008

Póczos, B., Xiong, L., Sutherland, D. J., & Schneider, J. 2012, in 2012 IEEE Conference on
        Computer Vision and Pattern Recognition, 2989

Press, W. H., Teukolsky, S. A., Vetterling, W. T., & Flannery, B. P. 1992, Numerical
        Recipes in C (2Nd Ed.): The Art of Scientific Computing (New York, NY, USA:
        Cambridge University Press)

Rodríguez-Torres, S. A., Chuang, C.-H., Prada, F., et al. 2016, Monthly Notices of the
        Royal Astronomical Society, 460, 1173

Roeder, K., & Wasserman, L. 1997, Journal of the American Statistical Association, 92, 894

Ross, A. J., Beutler, F., Chuang, C.-H., et al. 2017, Monthly Notices of the Royal
        Astronomical Society, 464, 1168

Schwarz, G. 1978, The Annals of Statistics, 6, 461

Scoccimarro, R. 1998, Monthly Notices of the Royal Astronomical Society, 299, 1097

—. 2000, The Astrophysical Journal, 544, 597

—. 2015, Physical Review D, 92, arXiv:1506.02729

Scott, D. W. 1992, Multivariate Density Estimation: Theory, Practice, and Visualization
        (Wiley)

Sellentin, E., Jaffe, A. H., & Heavens, A. F. 2017, arXiv:1709.03452 [astro-ph, stat],
        arXiv:1709.03452 [astro-ph, stat]

Sinha, M., Berlind, A. A., McBride, C. K., et al. 2017, arXiv:1708.04892 [astro-ph],
        arXiv:1708.04892 [astro-ph]

Slepian, Z., Eisenstein, D. J., Brownstein, J. R., et al. 2017, Monthly Notices of the Royal
        Astronomical Society, 469, 1738

Springel, V. 2005, Monthly Notices of the Royal Astronomical Society, 364, 1105

Steele, R. J., & Raftery, A. E. 2010

Taylor, E. N., Hopkins, A. M., Baldry, I. K., et al. 2015, Monthly Notices of the Royal Astronomical Society, 446, 2144

Tinker, J. L., & et al. in preparation

Vakili, M., & Hahn, C. H. 2016, arXiv:1610.01991 [astro-ph], arXiv:1610.01991 [astro-ph]

Vargas-Magaña, M., Ho, S., Xu, X., et al. 2014, Monthly Notices of the Royal Astronomical Society, 445, 2

Wang, Q., Sanjeev, K., & Sergio, V. 2009, IEEE TRANSACTIONS ON INFORMATION THEORY, 55, 2392

Wasserman, L. 2004, All of Statistics: A Concise Course in Statistical Inference (Springer Texts in Statistics) (Springer)

Wilkinson, D. M., Maraston, C., Thomas, D., et al. 2015, Monthly Notices of the Royal Astronomical Society, 449, 328

Wu, C. F. J. 1983, The Annals of Statistics, 11, 95

Zhao, C., Kitaura, F.-S., Chuang, C.-H., et al. 2015, Monthly Notices of the Royal Astronomical Society, 451, 4266

Zheng, Z., Coil, A. L., & Zehavi, I. 2007, The Astrophysical Journal, 667, 760

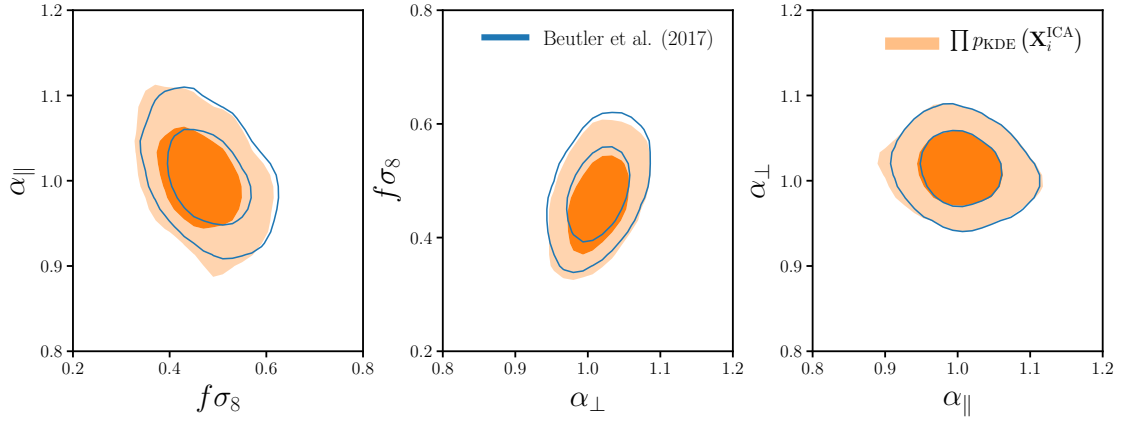Fig. 6.— Joint posterior distributions of $f\sigma_8$, $\alpha_\parallel$, and $\alpha_\perp$ in the B2017 P_ℓ analysis, compute using the non-Gaussian ICA likelihood (orange). We include, in blue, the original B2017 posteriors for comparison. The contours in the left and middle panels reflect the shift in $f\sigma_8$ caused by likelihood non-Gaussianity. Otherwise, the contours illustrate that likelihood non-Gaussianity has little impact on the cosmological parameters.
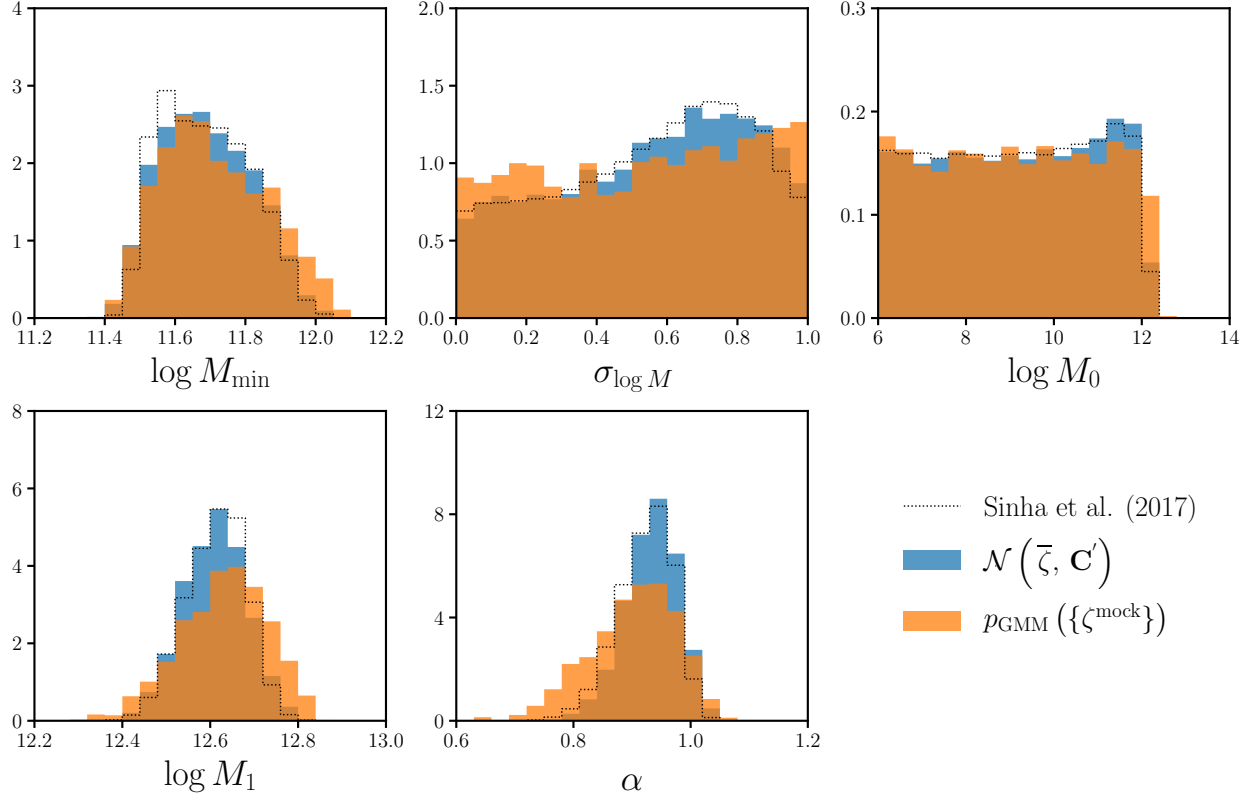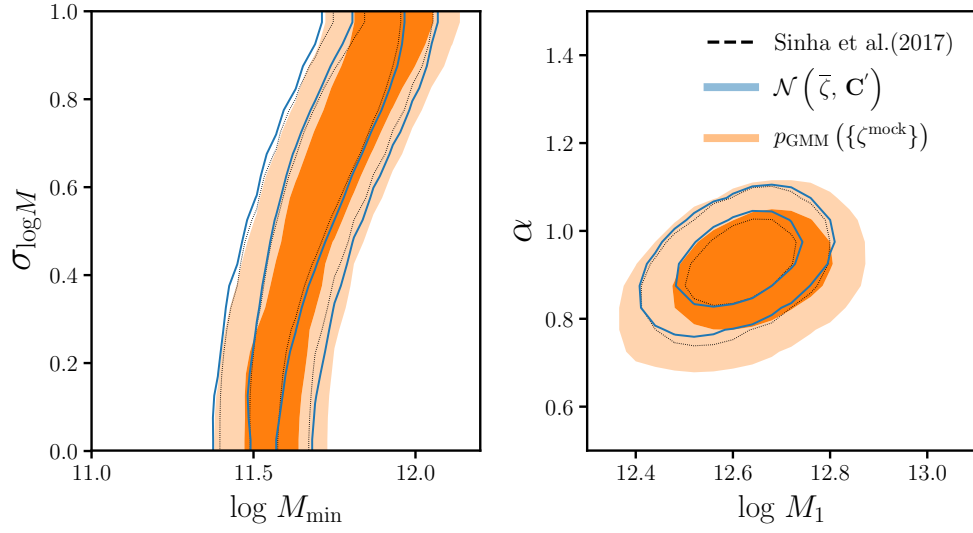
Fig. 7.—

Fig. 8.—